Journal of Biomechanics 46 (2013) 402–407

Contents lists available at SciVerse ScienceDirect

Journal of Biomechanics

journal homepage: www.elsevier.com/locate/jbiomech
www.JBiomech.com

High-resolution CFD detects high-frequency velocity fluctuations in bifurcation, but not sidewall, aneurysms ☆, ☆☆

Kristian Valen-Sendstad [a,b], Kent-André Mardal [b], David A. Steinman [a,*]

[a] Biomedical Simulation Laboratory, Department of Mechanical & Industrial Engineering, University of Toronto, 5 King's College Road, Toronto, Ontario, Canada M5S 3G8
[b] Center for Biomedical Computing, Simula Research Laboratory, P. O. Box 134, N-1325 Lysaker, Norway

ARTICLE INFO

Article history:
Accepted 26 October 2012

Keywords:
Intracranial aneurysm
Morphology
Hemodynamics
Rupture risk
Aneurysm type
Computational fluid dynamics

ABSTRACT

High-frequency flow fluctuations in intracranial aneurysms have previously been reported in vitro and in vivo. On the other hand, the vast majority of image-based computational fluid dynamics (CFD) studies of cerebral aneurysms report periodic, laminar flow. We have previously demonstrated that transitional flow, consistent with in vivo reports, can occur in a middle cerebral artery (MCA) bifurcation aneurysm when ultra-high-resolution direct numerical simulation methods are applied. The object of the present study was to investigate if such high-frequency flow fluctuations might be more widespread in adequately-resolved CFD models. A sample of $N=12$ anatomically realistic MCA aneurysms (five unruptured, seven ruptured), was digitally segmented from CT angiograms. Four were classified as sidewall aneurysms, the other eight as bifurcation aneurysms. Transient CFD simulations were carried out assuming a steady inflow velocity of 0.5 m/s, corresponding to typical peak systolic conditions at the MCA. To allow for detection of clinically-reported high-frequency flow fluctuations and resulting flow structures, temporal and spatial resolutions of the CFD simulations were in the order of 0.1 ms and 0.1 mm, respectively. A transient flow response to the stationary inflow conditions was found in five of the 12 aneurysms, with energetic fluctuations up to 100 Hz, and in one case up to 900 Hz. Incidentally, all five were ruptured bifurcation aneurysms, whereas all four sidewall aneurysms, including one ruptured case, quickly reached a stable, steady state solution. Energetic, rapid fluctuations may be overlooked in CFD models of bifurcation aneurysms unless adequate temporal and spatial resolutions are used. Such fluctuations may be relevant to the mechanobiology of aneurysm rupture, and to a recently reported dichotomy between predictors of rupture likelihood for bifurcation vs. sidewall aneurysms.

© 2012 Elsevier Ltd. All rights reserved.

1. Introduction

Treatment of intracranial aneurysms can be associated with risk to the patient (Wiebers et al., 2003), and so morphological discriminants beyond just size have been suggested to assess patient specific risk of aneurysm rupture (e.g., Xiang et al., 2011). These discriminants are quickly calculated from now-routine three-dimensional angiography, but are clearly surrogates for the complex forces that lead to structural alterations in the aneurysmal wall. Increasingly, computational fluid dynamics (CFD) simulations are used to describe the forces to which the arterial wall is exposed. The rationale has been to calculate the stresses on the wall in order to infer the strength of it, and hence the likelihood of aneurysm rupture.

The flow of blood in the *aneurysm sac* is often assumed to be laminar and relatively stable, since the Reynolds number (Re) in the *parent artery* is far below the commonly accepted threshold of $Re=2300$, where transition to turbulence occurs for steady pipe flow. Note that the critical Reynolds number is significantly reduced under pulsatile conditions, when flow is more likely to destabilize during deceleration (Peacock et al., 1998; Winter and Nerem, 1984). The numerical methods that are used are chosen or tailored according to these assumptions, i.e., to converge to a stable and laminar flow solution with the minimal amount of work (e.g., Cebral et al., 2011; Jou et al., 2008; Xiang et al., 2011).

☆ *Grant Support*: Canadian Institutes of Health Research, Operating Grant MOP-62934, to DAS; Research Council of Norway, Center of Excellence grant, to the Center for Biomedical Computing at Simula; Heart and Stroke Foundation of Canada, Career Investigator salary award, to DAS; Government of Canada, Postdoctoral research fellowship, to KVS.

☆☆ *Note*: Portions of this work have been presented in abstract form at the 1st International ECI Conference on CFD in Medicine and Biology (Ein Bokek, Israel, March 2012) and the 7th International Symposium on Biomechanics in Vascular Biology & Cardiovascular Disease (Atlanta GA, April 2012).

* Corresponding author. Tel.: +416 978 7781; fax: +416 978 7753.
E-mail address: steinman@mie.utoronto.ca (D.A. Steinman).

0021-9290/$ - see front matter © 2012 Elsevier Ltd. All rights reserved.
http://dx.doi.org/10.1016/j.jbiomech.2012.10.042

Table 1
Demographic, geometric, morphological and flow characteristics of the $N=12$ MCA aneurysms.

Case	Age	Sex	Status	Geometry type	D_{max} [mm]	D_{ostium} [mm]	D_{parent} [mm]	Aspect ratio	Size ratio	Flow type
1	57	M	Unruptured	Sidewall	7.15	6.03	2.33	1.15	3.04	Stable
2	63	F	Unruptured	Bifurcation	3.56	3.86	2.31	0.90	1.59	Stable
3	57	F	Ruptured	Bifurcation	3.49	3.38	1.89	1.80	3.61	Unstable
5	51	F	Unruptured	Sidewall	3.27	3.16	1.96	1.42	3.08	Stable
8	54	F	Unruptured	Sidewall	2.74	2.82	2.05	1.08	1.54	Stable
9	35	M	Ruptured	Bifurcation	3.43	3.56	1.83	0.79	1.58	Unstable
11	65	M	Ruptured	Bifurcation	10.0	9.19	2.72	1.00	3.95	Unstable
12	82	F	Ruptured	Bifurcation	7.71	6.69	2.00	0.94	3.86	Unstable
15	72	F	Ruptured	Sidewall	3.03	3.12	1.87	2.10	3.74	Stable
16	74	F	Ruptured	Bifurcation	8.24	7.91	2.09	0.80	3.32	Unstable
18	52	F	Ruptured	Bifurcation	3.62	3.64	1.37	0.59	1.65	Stable
20	57	M	Unruptured	Bifurcation	7.05	3.94	1.53	2.25	5.85	Stable

However, the literature contains much evidence, both in vivo (e.g., Ferguson, 1970; Kurokawa et al., 1994) and in vitro (e.g., Roach et al., 1972; Stehbens, 1975; Steiger and Reulen, 1986), supporting that certain aneurysms exhibit high-frequency flow fluctuations characteristic of laminar vortex shedding, transitional or turbulent flow. This seems to have been ignored, or at least has not received much attention, in the computational modeling community, resulting in an inconsistency between the clinically reported frequencies and their absence in published CFD studies.

Even though recent laminar CFD studies can discriminate between ruptured and unruptured aneurysms better than, e.g., aneurysm size (Cebral et al., 2011; Xiang et al., 2011), it is still not clear what are the links among the proposed hemodynamic agonists, their morphological surrogates, and the mechanisms of rupture (Baharoglu et al., 2012; Macdonald, 2012). Towards improved rupture risk indicators and a better understanding of the mechanobiology of aneurysm wall degradation, it seems important to resolve clinically reported high-frequency flow fluctuations and resulting flow structures. Previously we used ultra-high resolution direct numerical simulations (DNS) to fully resolve transitional flow in an anatomically realistic middle cerebral artery (MCA) bifurcation aneurysm (Valen-Sendstad et al., 2011). In the present study, we used spatially and temporally well-resolved CFD simulations to determine whether such unstable flow might be present beyond that single case study.

2. Methods

2.1. Patients and imaging

The original cohort consisted of the first 20 patients with middle cerebral artery (MCA) aneurysms treated at the Department of Neurosurgery, University Hospital of North Norway from 2006 to 2008. Three-dimensional (3D) imaging of the intracranial arteries and the aneurysms were obtained by CT angiography on a 16 multi-detector row spiral scanner (Somatom Sensation 16; Siemens, Erlangen, Germany), with spatial resolution of 0.3–0.5 mm. The register was approved by the local ethics committee and data inspectorate, and included patients gave informed consent. Of the 20 aneurysms, two were excluded by a neurosurgeon because of inconclusive clinical data, and six could not be reliably segmented and/or meshed, leaving $N=12$ aneurysms (five unruptured, seven ruptured) for hemodynamic analysis.

2.2. Geometry characterization

Aneurysms and surrounding arteries were digitally segmented from the CT angiograms using the gradient-based level set segmentation tools available from the open-source Vascular Modelling ToolKit (VMTK) (Antiga et al., 2008). High-frequency surface features were then smoothed using VMTK's volume-preserving Taubin filter.

Although all 12 aneurysms arose at or near MCA bifurcations, four were classified as sidewall aneurysms, as they did not arise at the apex of a bifurcation. The aneurysm ostium and sac were automatically identified from the segmented lumen surfaces and used to automatically compute the following geometric and morphological parameters (Piccinelli et al., 2012): maximum aneurysm diameter (D_{max}); mean diameter of the ostium plane (D_{ostium}); mean diameter of the parent artery (D_{parent}); aspect ratio (AR), the sac centerline length divided by D_{ostium}; and size ratio (SR), the sac centerline length divided by D_{parent}. Demographic and geometric characteristics of the 12 MCA aneurysms are summarized in Table 1.

2.3. Computational fluid dynamics

To solve the transient 3D Navier–Stokes equations we employed an incremental pressure correction scheme with Adams–Bashforth treatment of the convective term, and Crank–Nicolson discretization for the diffusive term. The solver employs first order linear elements for velocity and pressure, and is second order accurate in time (Mortensen et al., 2010). We assumed rigid walls, blood density of 1.025 g/cm^3 and blood viscosity of 0.035 Poise.

Aneurysms were recreated as a computational mesh using VMTK, including as much as possible from the surrounding arteries. The inlet and outlet vessels were extended by 10 diameters to reduce the effects of boundary artifacts. Meshes employed tetrahedral cells, concentrated in the aneurysmal region with an overall average side length of 0.10 mm, and three layers of boundary cells were used to resolve near-wall regions. Owing to a 10-fold variation in CFD model volumes (i.e., a 1000-fold variation in the number of elements if the same side lengths were used for all cases), the average side length was adjusted between 0.07 and 0.14 mm. This resulted in meshes ranging from 1.2 to 3.1 million elements, with an average mesh having 1.8 million elements. The time-step size for each case was chosen based on the mesh side length and inflow velocity, resulting in an average time step of 0.069 ms (range: 0.052–0.105 ms).

A uniform inflow velocity of $U=0.5$ m/s, with no fluctuating component, was imposed for each case, corresponding to peak systolic conditions at the MCA M1 segment (Krejza et al., 2005). Resistance conditions were applied at the outlets to ensure a physiologically balanced flow division (Alastruey et al., 2007). Steady inflow boundary condition (but solving the transient Navier–Stokes equations) was chosen for conceptual and computational tractability, since the goal was to identify the possibility of flow fluctuations rather than attempt to characterize patient-specific transitional or turbulent flow characteristics. Imposing the same inlet velocity for all cases presumes that flow rate scales with lumen area, which is consistent with optimality principles for larger arteries (Weinberg and Ethier, 2007; Zamir, 2000). The average parent artery Reynolds number was 292 (range: 201–398), based on D_{parent} and the prescribed blood properties and velocity. Simulations were initialized with zero velocity and pressure, and run for 10 'flow-throughs' (average: 424 ms; range: 266–581 ms), based on the extent of the computational domain divided by the inflow velocity. A separate set of simulations was carried out with $U=0.6$ m/s, to test the sensitivity of the results to the choice of inflow velocity.

2.4. Flow characterization

Instantaneous velocities in each of the three directions (u_i) were decomposed into mean ($\overline{u_i}$) and fluctuating (u_i') components. After five initial 'flow-throughs' to wash out the effects of initial conditions, the remaining 5 were used to compute the turbulent kinetic energy (TKE), a standard measure of the mean square velocity fluctuation, i.e.,

$$TKE = \frac{1}{2}\left(\overline{(u_1')^2} + \overline{(u_2')^2} + \overline{(u_3')^2}\right)$$

We then classified flow into two groups: *stable*, where flow disturbances throughout the domain are dampened from the initial 'flow-throughs', with TKE $< 10^{-4}$ m^2/s^2; and *unstable*, where flow exhibits a continuation or amplification

of disturbances, possibly including random and rapid fluctuations in space and time at a continuous range of frequencies.

3. Results

Fig. 1 shows maps of TKE for the 12 cases; cases without fluctuations appear empty. Flow in all four sidewall aneurysms was stable (Cases #1,5,8,15), whereas five of the eight bifurcation aneurysms (Cases #3,9,11,12,16) exhibited fluctuation energies above 10^{-4} m^2/s^2, and thus were classified as unstable. Frequency spectra (Fig. 2A) and velocity traces (Fig. 2B) give some insight into the nature of the fluctuations. Cases #3 and #16 experienced strong, high-frequency fluctuations, with spectra showing energetic contributions up to about 900 Hz and 300 Hz, respectively. Cases #11 and #12 demonstrated slightly weaker aperiodic fluctuations, albeit still with energetic contributions up to about 100 Hz. The weakly unstable Case #9, on the other hand, was characterized by a periodic fluctuation, suggestive of regular vortex shedding, at around 200 Hz. Fig. 2C shows how the initial transients were quickly damped out for the stable cases, except for sidewall Case #1, for which fluctuations were still decaying past 5 'flow throughs', but the TKE was well below 10^{-4} m^2/s^2. Increasing the inflow velocity by 20% (i.e., $U=0.6$ m/s) introduced weak but persistent low frequency (<10 Hz) fluctuations into this case, otherwise the flow classifications were unchanged.

As might be expected for this small sample, t tests revealed no significant differences ($p>0.05$) in D_{max}, D_{ostium}, D_{parent}, AR or SR for unruptured vs. ruptured aneurysms or stable vs. unstable flow cases, whether bifurcation types or pooled with sidewall types. There was also no significant difference in Reynolds number for stable vs. unstable flow cases. Referring to Table 1, however, an intriguing albeit incidental finding was that all five unstable cases were ruptured bifurcation aneurysms, whereas all four sidewall aneurysms, including one ruptured case, were stable.

4. Discussion

The present study has demonstrated that energetic velocity fluctuations at or above 100 Hz are likely a common occurrence in CFD models of intra-aneurysmal hemodynamics, provided care is taken to resolve them, or at least not to suppress them numerically. These fluctuations were isolated to bifurcation aneurysms, which is consistent with observations from in vitro studies. (Steiger and Reulen, 1986) They also occurred exclusively in ruptured aneurysms. This might be a coincidence since bifurcation aneurysms are more prone to rupture anyway, but interesting nonetheless in light of the dichotomy between sidewall and bifurcation aneurysms recently identified by Baharoglu et al. (2012). As discussed below,

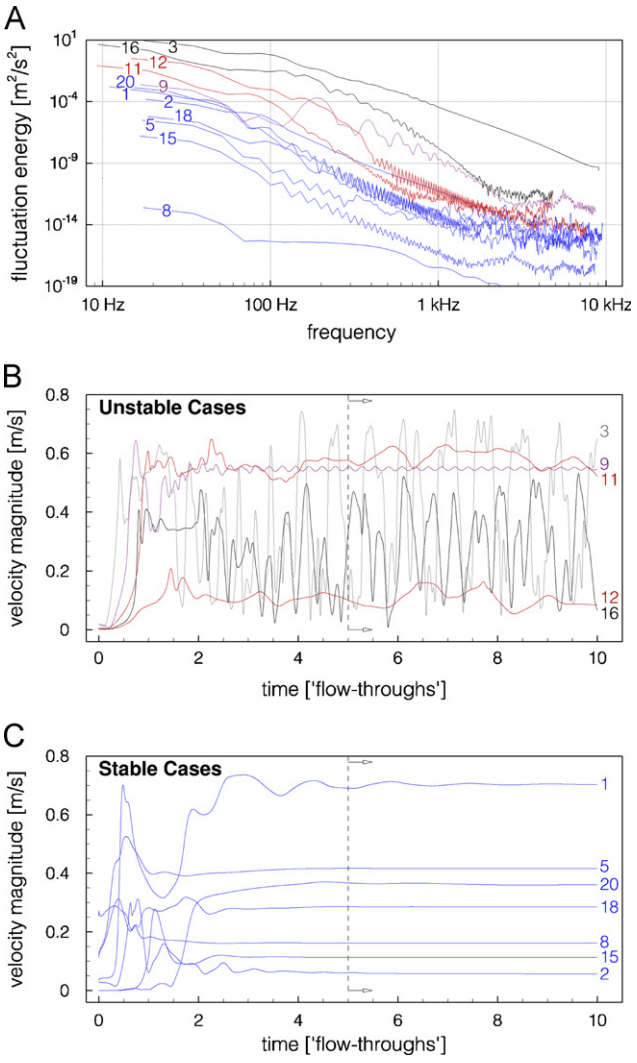

Fig. 2. (A) TKE spectra from a representative location within the sac for each case, and corresponding velocity traces for (B) unstable cases and (C) stable cases. The dashed line in panels B and C identifies the time after which the TKE analysis was started, i.e., 5 'flow-throughs'.

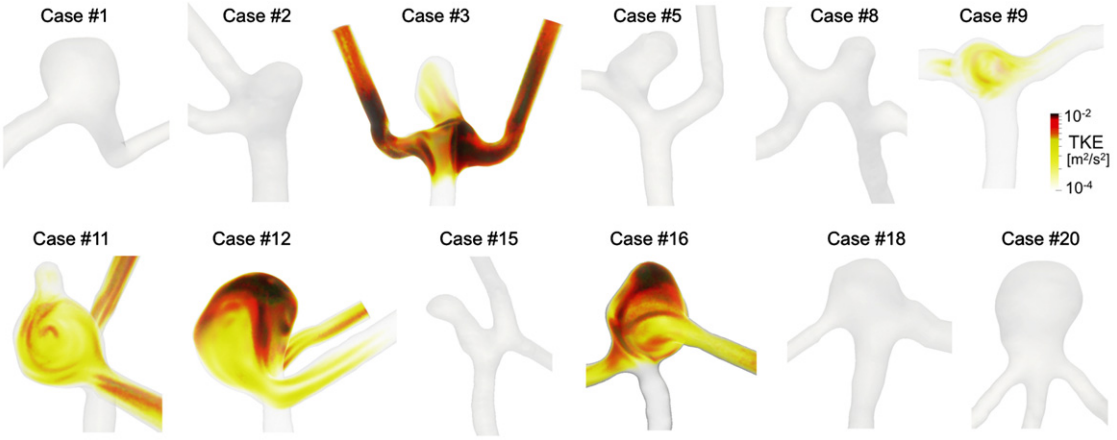

Fig. 1. Volume rendering of energy fluctuations (TKE, per the indicated legend). Individual panels are cropped to visualize the aneurysm sac and surrounding branches, and so are not necessarily to the same scale.

the presence of such flow fluctuations in bifurcation aneurysms, and their continued absence in the growing body of image-based CFD studies of aneurysm hemodynamics, has potential implications for understanding the mechanobiology of cerebral aneurysms, and for the identification of potential hemodynamic or morphological predictors of rupture risk.

4.1. Unstable flow and aneurysm pathophysiology

The literature is full of good evidence of the presence of high-frequency flow fluctuations in certain aneurysms. For example, bruits were found in 10 of 17 cases during craniotomy when a phonocatheter was applied to the exposed aneurysm sac (Ferguson, 1970), and 12 of 15 cases noninvasively at the eye (Kurokawa et al., 1994). In vitro studies have also demonstrated the presence of unstable flow in glass models of bifurcation aneurysms (Roach et al., 1972; Stehbens, 1975; Steiger and Reulen, 1986), although these observations have tended to be qualitative and/or limited to relatively low frequencies. It remains unclear whether these instabilities reflect truly transitional or turbulent flow, or are the signature of laminar vortex shedding, and the present study does not attempt to discriminate between the two. Rather, we would argue that the precise effects of such fluctuations – whatever their source – on mechanotransduction and gene expression may in fact be important in order to understand aneurysm wall degradation leading to aneurysm rupture. For example, high frequency velocity fluctuations can lead to strong spatial and temporal gradients in wall shear stress (Valen-Sendstad et al., 2011), which are known to elicit distinct cellular responses (e.g., Dolan et al., 2011; White et al., 2005).

Since inertial forces exceed viscous forces in certain aneurysm flows, nonlinear instabilities occur that may result in highly energetic fluctuations. There is a flux of energy that is transferred to continuously smaller eddies, at least down to dissipative scales. The impingement on the wall of the small scale eddies would be manifested by intricate wall shear stress (WSS) patterns that can change in magnitude and direction much faster than the heart beat (Valen-Sendstad et al., 2011). Such strong WSS gradients may well exceed those already implicated in vascular responses leading to aneurysm formation (Metaxa et al., 2010). Similarly, DNS of pulsatile flow in a MCA bifurcation aneurysm has revealed peak pressure fluctuations of 1–2 mmHg at 100 Hz (Valen-Sendstad et al., 2011), which, although negligible compared to the pulse pressure, may act upon such a small area that the pressure gradients at the wall could induce non-negligible radial shearing within the wall itself.

4.2. CFD modeling of aneurysm hemodynamics

Despite the above-mentioned indications of possible high-frequency flow fluctuations, most CFD studies of cerebral aneurysm hemodynamics are based on the implicit or explicit assumption of laminar flow (e.g., Cebral et al., 2011; Jou et al., 2008; Shojima et al., 2004; Xiang et al., 2011). The numerical methods and algorithms that are used to model the flow are chosen accordingly. They are often stabilized implicit iterative methods that introduce numerical diffusion and dampen the disturbances such that transition to unstable flow with high-frequency fluctuations is numerically suppressed. Additionally, spatial and temporal resolutions optimized for laminar flow phenomena would likely damp any small-scale or high-frequency flow structures such that the simulated flow is destined to appear stable. For example, and in contradistinction to the findings of the present study, a landmark CFD study of 20 MCA aneurysms reported no flow instability (Shojima et al., 2004). Only three of the cases were ruptured; however, the reported spatial resolution (60,000 hexahedral elements, roughly equivalent to 300,000 tetrahedra vs. an average of 1.8 million tetrahedra in the present study) was probably insufficient to detect flow instabilities if present, and the authors explicitly noted that they stabilised the scheme to dampen flow disturbances, since they assumed blood flow to be laminar. Numerical suppression of high frequency velocity fluctuations could lead to a underestimation of WSS spatial and temporal gradients, and hence a mischaracterization of the mechanobiological stimuli that may be important to understand aneurysm growth and rupture.

Similarly, leading groups in aneurysm hemodynamics research are not only using stabilised numerical methods, but also report using 100–1000 time steps per second, in contrast to roughly 15,000 time steps per second in the present study, or 40,000 when all the spatial and temporal scales of transitional flow were shown to be resolved (Valen-Sendstad et al., 2011). In principle our simulations allowed for the detection of frequencies up to about 5 kHz. In practice we observed non-negligible fluctuations up to about 900 Hz (Case #3). The effect of the reduced resolution can be seen in Case #16, which was also the case studied earlier under pulsatile flow conditions by DNS. In the current simulation, flow in that particular aneurysm contained energetic fluctuations up to about 300 Hz, which is in contrast to 1250 Hz by DNS (Valen-Sendstad et al., 2011); however, we did not attempt or intend to fully resolve the smallest temporal or spatial scales, but rather the scales with the most energy.

Admittedly, ours is not the first study to detect unstable flow in cerebral aneurysm CFD models. Valencia (2005) reported low frequency (<10 Hz) laminar fluctuations in an idealized basilar tip aneurysm model; however, the artificial symmetry of such models may be inherently more conducive to flow instabilities (Steinman et al., 2003). For anatomically realistic aneurysms, the presence of unstable flow was first hinted at by Ford et al. (2008), who reported persistent cycle-to-cycle fluctuations in a basilar tip aneurysm case, but not a (sidewall) ICA case. Later, high resolution CFD of three sidewall ICA aneurysms was performed by Baek et al. (2009), although no unstable high-frequency flow fluctuations was reported, only relatively low-frequency laminar fluctuations (<50 Hz). Additionally, those authors reported that the flow patterns were repeated every cycle, which contrasts the cycle-to-cycle differences found by Ford et al., and in our previous DNS study (Valen-Sendstad et al., 2011). It seems likely, however, that there were no high-frequency fluctuations because the specific aneurysms were of small/medium size and sidewall aneurysms, where the kinetic energy is generally low. Unstable flow was not found in any of the sidewall aneurysms considered in the present study, except for one case at the higher flow rate, and then only at low frequencies.

4.3. Hemodynamic and morphological predictors of rupture risk

Low levels of WSS have been related to aneurysm rupture (Jou et al., 2008; Xiang et al., 2011; Yasuda et al., 2011), but also have concentrated inflow and impingement (Cebral et al., 2011), which implicates high WSS and WSS gradients. This suggests that the complex processes associated with aneurysm growth and rupture remain mostly unclear. Searching for one universal index to discriminate aneurysm rupture may be inappropriate when both too-high and too-low WSS are known to be damaging to the endothelial cells. There may well be different processes related to rupture in aneurysms where the WSS and energy are low (Xiang et al., 2011; Yasuda et al., 2011) vs. aneurysms with high energy and dynamic WSS such as in the current study or Castro et al. (2009).

Evidence for such a potential dichotomy has emerged recently in a report by Baharoglu et al. (2012) who demonstrated that the

rupture status of sidewall aneurysms was associated with size and shape parameters previously proposed as rupture risk indicators, whereas those parameters fared poorly for predicting the rupture status of bifurcation aneurysms. Bearing in mind that such parameters are, ultimately, surrogates of the more-difficult-to-measure hemodynamics factors putatively linked to the biophysical mechanisms of aneurysm rupture, it stands to reason that the success of such parameters depends on a thorough understanding of the hemodynamic factors they purport to represent. The absence of unstable flow in sidewall aneurysms in our study suggests that their hemodynamics may be well represented by the majority of CFD studies, whereas the same may not be said for bifurcation aneurysms. A more complete understanding of the hemodynamics in bifurcation aneurysms, accounting for unstable laminar or possibly turbulent flow, may be necessary before satisfactory morphological or hemodynamic discriminants can be identified.

4.4. Assumptions and potential limitations

The use of a steady inflow at peak systolic conditions is obviously a key simplifying assumption, but was a pragmatic choice to isolate the sum of geometrical factors that promote high-frequency velocity fluctuations. Under pulsatile flow conditions, such fluctuations would cause the bulk flow pattern to lose coherence as flow begins to decelerate. In fact, this was demonstrated for Case #16, which here showed a transient response to stationary inflow conditions, and which was previously shown to exhibit transitional flow under pulsatile flow conditions (Valen-Sendstad et al., 2011). On the other hand, adequate resolution of all scales of the unstable aneurysmal flow under pulsatile flow conditions required 5500 CPU-hours (Valen-Sendstad et al., 2011). Such simulations are impractical for a larger group of patients or eventual clinical application, and so we reduced the models from transient to stationary, and averaged over 'flow-throughs' rather than cardiac cycles. This resulted in a computational savings of more than 99%, while still allowing us to detect the likelihood of (c.f., fully resolve) high-frequency fluctuations.

In the absence of patient-specific flow rates, we were also forced to prescribe representative velocity conditions, albeit consistent with previously reported values and accepted scaling principles. As a result, we cannot say with certainty what are the patient-specific flow conditions – this was not our intent anyway – but rather that for an equal velocity magnitude and resistance outflow boundary conditions, 5 of 8 MCA bifurcation aneurysms had a morphology that gave rise to unstable, high-frequency flow fluctuations in response to stationary inflow conditions. We also made the usual assumption of rigid walls, based on the fact that realistic computational models have suggested that the wall deformation is negligible (Zhao et al., 2011), and that turbulence-induced wall vibration has been shown to be at the order of microns in a comparable experiment of an arteriovenous graft (Lee et al., 2005). Constant (Newtonian) blood viscosity was assumed, to be consistent with the vast majority of aneurysm CFD studies; and anyway conventional non-Newtonian models may be of questionable applicability in the presence of high-frequency fluctuations (Antiga and Steinman, 2009).

As with virtually all image-based CFD studies, our study was necessarily retrospective and, owing to its small size, likely subject to selection bias. We are also aware that any image-based CFD study is dependent upon a correct interpretation of the underlying images. For example, neck size may be overestimated by CTA (Brinjikji et al., 2009); however, since unstable flow is likely related to the concentration of momentum at the neck, the implication for our study would be that unstable, high-frequency flow fluctuations have, if anything, been underestimated in the current simulations.

5. Conclusions

Unstable, high-frequency velocity fluctuations in aneurysms may be as common as stable, laminar flow, at least in bifurcation types. This has been shown in vivo, in vitro, and, for the first time, computationally. When properly resolved, CFD can be used to detect these instabilities and their implications for the pathophysiology of cerebral aneurysms, perhaps leading to new and better morphological or hemodynamic predictors of rupture risk. At the same time, some of the ongoing confusion in the literature regarding such risk factors may have its origins in an incomplete understanding of aneurysm hemodynamics, attributable to an overabundance of under-resolved CFD studies in the literature.

Conflict of interest statement

The authors have no conflicts of interest to declare.

Acknowledgments

We thank Neurosurgeon Dr. Jørgen Isaksen for providing the medical images and for verification of the segmented aneurysms.

References

Alastruey, J., Parker, K.H., Peiro, J., Byrd, S.M., Sherwin, S.J., 2007. Modelling the circle of Willis to assess the effects of anatomical variations and occlusions on cerebral flows. Journal of Biomechanics 40, 1794–1805.
Antiga, L., Piccinelli, M., Botti, L., Ene-Iordache, B., Remuzzi, A., Steinman, D.A., 2008. An image-based modeling framework for patient-specific computational hemodynamics. Medical & Biological Engineering & Computing 46, 1097–1112.
Antiga, L., Steinman, D.A., 2009. Rethinking turbulence in blood. Biorheology 46, 77–81.
Baek, H., Jayaraman, M.V., Richardson, P.D., Karniadakis, G.E., 2009. Flow instability and wall shear stress variation in intracranial aneurysms. Journal of the Royal Society Interface 7, 967–988.
Baharoglu, M.I., Lauric, A., Gao, B.L., Malek, A.M., 2012. Identification of a dichotomy in morphological predictors of rupture status between sidewall- and bifurcation-type intracranial aneurysms. Journal of Neurosurgery 116, 871–881.
Brinjikji, W., Cloft, H., Lanzino, G., Kallmes, D.F., 2009. Comparison of 2D digital subtraction angiography and 3D rotational angiography in the evaluation of dome-to-neck ratio. American Journal of Neuroradiology 30, 831–834.
Castro, M.A., Putman, C.M., Sheridan, M.J., Cebral, J.R., 2009. Hemodynamic patterns of anterior communicating artery aneurysms: a possible association with rupture. American Journal of Neuroradiology 30, 297–302.
Cebral, J.R., Mut, F., Weir, J., Putman, C.M., 2011. Association of hemodynamic characteristics and cerebral aneurysm rupture. American Journal of Neuroradiology 32, 264–270.
Dolan, J.M., Meng, H., Singh, S., Paluch, R., Kolega, J., 2011. High fluid shear stress and spatial shear stress gradients affect endothelial proliferation, survival, and alignment. Annals of Biomedical Engineering 39, 1620–1631.
Ferguson, G.G., 1970. Turbulence in human intracranial saccular aneurysms. Journal of Neurosurgery 33, 485–497.
Ford, M.D., Nikolov, H.N., Milner, J.S., Lownie, S.P., Demont, E.M., Kalata, W., Loth, F., Holdsworth, D.W., Steinman, D.A., 2008. PIV-measured versus CFD-predicted flow dynamics in anatomically realistic cerebral aneurysm models. Journal of Biomechanical Engineering 130, 021015.
Jou, L.D., Lee, D.H., Morsi, H., Mawad, M.E., 2008. Wall shear stress on ruptured and unruptured intracranial aneurysms at the internal carotid artery. American Journal of Neuroradiology 29, 1761–1767.
Krejza, J., Szydlik, P., Liebeskind, D.S., Kochanowicz, J., Bronov, O., Mariak, Z., Melhem, E.R., 2005. Age and sex variability and normal reference values for the V(MCA)/V(ICA) index. American Journal of Neuroradiology 26, 730–735.
Kurokawa, Y., Abiko, S., Watanabe, K., 1994. Noninvasive detection of intracranial vascular lesions by recording blood flow sounds. Stroke 25, 397–402.
Lee, S.W., Fischer, P.F., Loth, F., Royston, T.J., Grogan, J.K., Bassiouny, H.S., 2005. Flow-induced vein-wall vibration in an arteriovenous graft. Journal of Fluid Structure 20, 837–852.

Macdonald, R.L., 2012. Editorial: on the persisting difficulty of making predictions, especially about the future. Journal of Neurosurgery 116 (866-869), 869–870, discussion.

Metaxa, E., Tremmel, M., Natarajan, S.K., Xiang, J., Paluch, R.A., Mandelbaum, M., Siddiqui, A.H., Kolega, J., Mocco, J., Meng, H., 2010. Characterization of critical hemodynamics contributing to aneurysmal remodeling at the basilar terminus in a rabbit model. Stroke 41, 1774–1782.

Mortensen, M., Mardal, K.A., Langtangen, H.P., 2010. Simulations of transitional flow. In: Logg, A., Mardal, K.A., Wells, G.N. (Eds.), Automated Scientific Computing. Springer-Verlag, pp. 397–414.

Peacock, J., Jones, T., Tock, C., Lutz, R., 1998. The onset of turbulence in physiological pulsatile flow in a straight tube. Experiments in Fluids 24, 1–9.

Piccinelli, M., Steinman, D.A., Hoi, Y., Tong, F., Veneziani, A., Antiga, L., 2012. Automatic neck plane detection and 3D geometric characterization of aneurysmal sacs. Annals of Biomedical Engineering 40, 2188–2211.

Roach, M.R., Scott, S., Ferguson, G.G., 1972. The hemodynamic importance of the geometry of bifurcations in the circle of Willis (glass model studies). Stroke 3, 255–267.

Shojima, M., Oshima, M., Takagi, K., Torii, R., Hayakawa, M., Katada, K., Morita, A., Kirino, T., 2004. Magnitude and role of wall shear stress on cerebral aneurysm: computational fluid dynamic study of 20 middle cerebral artery aneurysms. Stroke 35, 2500–2505.

Stehbens, W.E., 1975. Flow in glass models of arterial bifurcations and berry aneurysms at low Reynolds numbers. Quarterly Journal of Experimental Physiology and Cognate Medical Sciences 60, 181–192.

Steiger, H.J., Reulen, H.J., 1986. Low frequency flow fluctuations in saccular aneurysms. Acta Neurochirurgica (Wien) 83, 131–137.

Steinman, D.A., Kehoe, S.C., Ford, M.D., Nikolov, H.N., Holdsworth, D.W., 2003. Dancing on the knife-edge of symmetry: on the misuse of symmetric models for studying blood flow dynamics. In: Proceedings of ASME Bioengineering Conference, Key Biscayne, FL.

Valen-Sendstad, K., Mardal, K.A., Mortensen, M., Reif, B.A., Langtangen, H.P., 2011. Direct numerical simulation of transitional flow in a patient-specific intracranial aneurysm. Journal of Biomechanics 44, 2826–2832.

Valencia, A., 2005. Simulation of unsteady laminar flow in models of terminal aneurysm of the basilar artery. International Journal of Computational Fluid Dynamics 19, 337–345.

Weinberg, P., Ethier, C.R., 2007. Twenty-fold difference in hemodynamic wall shear stress between murine and human aortas. Journal of Biomechanics 40, 1594–1598.

White, C.R., Stevens, H.Y., Haidekker, M., Frangos, J.A., 2005. Temporal gradients in shear, but not spatial gradients, stimulate ERK1/2 activation in human endothelial cells. American Journal of Physiology Heart and Circulatory Physiology 289, H2350–2355.

Wiebers, D.O., Whisnant, J.P., Huston III, J., Meissner, I., Brown Jr., R.D., Piepgras, D.G., Forbes, G.S., Thielen, K., Nichols, D., O'Fallon, W.M., Peacock, J., Jaeger, L., Kassell, N.F., Kongable-Beckman, G.L., Torner, J.C., 2003. Unruptured intracranial aneurysms: natural history, clinical outcome, and risks of surgical and endovascular treatment. Lancet 362, 103–110.

Winter, D.C., Nerem, R.M., 1984. Turbulence in pulsatile flows. Annals of Biomedical Engineering 12, 357–369.

Xiang, J., Natarajan, S.K., Tremmel, M., Ma, D., Mocco, J., Hopkins, L.N., Siddiqui, A.H., Levy, E.I., Meng, H., 2011. Hemodynamic-morphologic discriminants for intracranial aneurysm rupture. Stroke 42, 144–152.

Yasuda, R., Strother, C.M., Taki, W., Shinki, K., Royalty, K., Pulfer, K., Karmonik, C., 2011. Aneurysm volume-to-ostium area ratio: a parameter useful for discriminating the rupture status of intracranial aneurysms. Neurosurgery 68 (310–317), 317–318, discussion.

Zamir, M., 2000. The Physics of Pulsatile Flow. American Institute of Physics, Melville, NY.

Zhao, X., Raghavan, M.L., Lu, J., 2011. Characterizing heterogeneous properties of cerebral aneurysms with unknown stress-free geometry: a precursor to in vivo identification. Journal of Biomechanical Engineering 133, 051008.